Malaysian Journal of Chemistry, 2026, Vol. 28(2), 48-57

Thermal Management during Exothermic Hydrogenation of Metal Hydride using Phase Change Materials of Varying Thicknesses

Ying Xu[1], Murray McCurdy[2], Fei Yang[1]* and Mohammed Farid[3]*

[1]Waikato Centre for Advanced Materials and Manufacturing, School of Engineering Teaching and Research, The University of Waikato, Hamilton 3240, New Zealand

[2]Department of Earth Resources and Materials, Earth Sciences New Zealand, Lower Hutt 5010, New Zealand

[3]Phase Foam Ltd, Auckland 1071, New Zealand

*Corresponding author (e-mail: mohammed.farid@phasefoam.com and fei.yang@waikato.ac.nz)

Metal hydrides (MHs) are a promising medium for hydrogen storage due to their high gravimetric and volumetric capacities, as well as inherent safety advantages. However, the exothermic nature of hydrogen absorption presents significant thermal management challenges. Effective heat dissipation is critical to maintain optimal thermodynamic and kinetic conditions and ensure system safety. Integrating phase change materials (PCMs) into a metal hydride system offers a passive strategy for thermal regulation. This study systematically investigated how the thickness of a compressed expanded graphite-based composite PCM layer influenced thermal performance during MH hydrogenation. Variable-power electrical heating was employed to simulate the heat generated during the hydrogenation of lanthanum–nickel, based on its reported reaction kinetics and thermodynamic properties. Increasing the composite PCM thickness enhanced thermal buffering and reduced peak temperatures, whereas excessive thickness increased thermal resistance and decreased overall efficiency. A 5.0 mm PCM layer provided an optimal balance of heat transfer, latent heat storage, thermal management, and operational safety, supporting a compact and cost-effective system under the simulated conditions.

Keywords: Metal hydride, phase change material, compressed expanded graphite composite, heat dissipation, thermal management, hydrogenation, thermal buffering

Received: September 2025; Accepted: November 2025

Growing global energy demand is driving the search for sustainable energy production and storage [1]. Hydrogen has emerged as a promising clean energy carrier and secondary energy source for the future due to its high gravimetric energy density (120 MJ kg^{-1}), versatility, and zero-emission combustion. Despite its benefits, hydrogen energy faces challenges, with safe, efficient, and scalable hydrogen storage being a major hurdle [2, 3, 4, 5].

Conventional physical storage methods, such as compressed gas, cryo-compressed hydrogen, and liquid hydrogen, require either high-pressure tanks or cryogenic temperatures. These conditions impose significant technical complexity, safety concerns, and cost burdens. Consequently, material-based hydrogen storage systems, such as metals and alloys, complex metal hydrides, and metal–organic frameworks (MOFs), have gained increasing attention as potential alternatives because of their advantages such as high volumetric and gravimetric hydrogen densities, moderate operating conditions, and improved safety profiles [6, 7, 8, 9].

Among these, metal hydrides (MHs) represent one of the most promising solid-state hydrogen storage media owing to their favourable reversibility and high hydrogen capacity [10, 11, 12, 13]. However, the hydrogen absorption and desorption processes in MHs are highly exothermic and endothermic, respectively, making thermal management critical to system performance [14, 15, 16, 17]. Because their performance is strongly temperature-dependent, effective thermal management is essential to maintain favourable thermodynamic and kinetic conditions, ensure cycling efficiency and guarantee system safety. Over the past decades, extensive experimental and numerical studies have investigated various reactor geometries, heat exchanger configurations, and strategies to enhance thermal conductivity [17, 18, 19, 20, 21, 22]. Recently, increasing attention has been directed toward the integration of phase change materials (PCMs) as an effective approach for thermal regulation [23, 24, 25].

PCMs are a promising solution for thermal regulation in MH systems due to their ability to absorb

or release significant amounts of latent heat at nearly constant temperatures. [23, 24, 25]. PCMs are classified into two main categories: inorganic and organic. Inorganic PCMs, such as salts, salt hydrates, and metals, generally offer higher latent heat capacities. However, their corrosiveness, toxicity and high cost limit their applicability in MH storage systems. Organic PCMs, including paraffins, glycols, and fatty acids, are widely used in low- to medium-temperature applications due to their chemical stability, adjustable melting points, high latent heat capacities, and cost-effectiveness. Nevertheless, their inherently low thermal conductivity and poor shape stability hinder heat transfer, limiting their suitability for high heat-flux environments like MH storage systems [23, 24, 25].

To overcome the limitations of organic PCMs, several strategies have been developed to enhance their thermal performance and structural stability. One widely adopted method involves incorporating highly conductive additives such as metal particles, metal foams, carbon nanotubes (CNTs) or graphite, into the PCM matrix [23, 25, 26, 27, 28]. These additives create efficient heat transfer pathways, therefore improving thermal conductivity and facilitating uniform heat distribution during phase transitions. In parallel, shape stabilization and encapsulation techniques have been employed to address leakage and mechanical degradation. These approaches involve embedding PCMs within porous supports (e.g., expanded graphite or silica aerogels) or encapsulating them in polymeric, or ceramic shells. Such configurations not only prevent leakage but also enhance mechanical integrity and long-term cycling stability [26, 27, 28, 29, 30, 31].

Composite PCMs, which integrate thermally conductive networks within shape-stabilized matrices, have demonstrated significant effectiveness in enhancing thermal regulation. Among these, compressed expanded graphite-based composite PCMs are particularly notable due to their high thermal conductivity, chemical compatibility, and porous structure, which facilitate uniform organic PCM dispersion and retention [26, 32].

In addition to composition, the thickness of the PCM layer plays a critical role in the performance of MH systems. Thicker PCM layers improve thermal buffering and help mitigate peak temperatures. However, excessive thickness can lead to increased thermal resistance, reduced heat utilization efficiency, greater reactor volume occupation, and elevated cost [24, 33,34]. Hence, optimizing PCM thickness is crucial for achieving efficient and balanced thermal management.

In our previous work, a compressed expanded graphite-based composite PCM was developed for potential integration into a metal hydride reactor operating within the temperature range of 290–340 K under near-atmospheric pressure [26]. The composite combined a selected paraffin-based PCM with compressed expanded graphite to enhance its thermal conductivity while maintaining a high energy storage capacity.

This study systematically investigates how the thickness of a compressed expanded graphite-based composite PCM layer influences the thermal performance during the hydrogenation process. Composite PCM samples with thicknesses of 2.5 mm, 5.0 mm, and 10.0 mm were sectioned from a single, uniformly compressed expanded graphite block to ensure material consistency. The thermophysical properties of these samples were characterized, and their heat transfer performance was evaluated under conditions simulating the exothermic hydrogenation of $LaNi_5$, a commercially available alloy known for its rapid activation and high hydrogen absorption capacity under the target operating conditions [35]. To replicate the thermal environment associated with $LaNi_5$ hydrogenation, an electric heater equipped with an adjustable and programmable power control was employed.

EXPERIMENTAL

Materials

Compressed expanded graphite blocks were sourced from Duranice Applied Materials (Dalian, China), and paraffin wax (PCM38) was obtained from Shanghai Ru Entropy New Energy Technology Co. Ltd (China). The paraffin, with a melting point of 36–38 °C and a latent heat of 226 kJ/kg, served as the phase change material (PCM).

Preparation of Composite PCMs

Compressed expanded graphite-based composite PCMs were prepared via direct impregnation. The graphite matrix with thicknesses of 2.5 mm, 5.0 mm, and 10.0 mm were precisely sectioned from a single, uniformly compressed expanded graphite block using a thin precision cutting blade to ensure material consistency. The thickness of each matrix was measured with digital callipers.

The prepared graphite matrices were then submerged in molten paraffin (PCM38) under atmospheric pressure using a controlled-temperature water bath maintained at 40 °C. The impregnation process was conducted over 18 hours to ensure complete saturation of the porous graphite structure. Following impregnation, the samples were transferred to a drying oven and held at 50 °C for 10 minutes to remove any excess surface paraffin. The thicknesses of the as-prepared composite PCMs were re-measured to ensure final sample thicknesses of 2.5 mm, 5.0 mm, and 10.0 mm, with an accuracy of ±0.05 mm. The

slight volume expansion observed after impregnation was limited and therefore regarded as negligible. Then, the as-prepared composite PCMs were used for subsequent thermal performance evaluation.

The PCM absorption percentage was determined based on the mass increase of the graphite matrix following impregnation (Equation 1). This value was subsequently used to calculate the theoretical latent heat values of the composite PCMs.

$$\%PCM = \frac{m_1 - m_0}{m_1} \times 100 \quad (1)$$

Where:

-m_1 is the mass of composite PCM

-m_0 is the mass of the graphite matrix

Characterization Methods

The morphologies and microstructures of the cross-sectional compressed expanded graphite matrix and the prepared composite PCMs were analysed using a scanning electron microscope (SEM, JEOL JSM-6500). The SEM images were captured at an accelerating voltage of 15 kV to examine the PCM distribution and pore structure.

The thermal properties of the samples were characterized using differential scanning calorimetry (DSC, NETZSCH DSC3500) over a temperature range of -10 °C to 70 °C. Measurements were conducted at a heating/cooling rate of 0.5 °C/min under a constant nitrogen flow. To ensure thermal equilibrium, an isothermal hold of 5 minutes was applied at the end of each heating and cooling stage.

A custom thermal performance apparatus (Figure 1) was developed to conduct two types of experiments. The setup applied a controlled heat input to the composite PCM and measured its thermal response. Heat was supplied via a small flat cartridge heater (2 cm × 2 cm), powered by a programmable DC power supply. A composite PCM sample of specified thickness and matching lateral dimensions to the flat heater was placed directly on top of the heater and heated from the bottom surface. All other sides were insulated to ensure approximate one-dimensional heat flow through the PCM. The thermal response was defined by the temperature variation over time at the interface temperature, T_m, located between the cartridge heater and the composite PCM (Figure 1). This temperature was measured using a K-type thermocouple (0.5 mm in diameter) embedded in the composite PCMs and recorded via a data logger connected to a computer.

The first experimental setup was designed to measure the thermal response of composite PCM under a constant heat flow. In this configuration, full-size composite PCM samples were subjected to a steady heat flux generated by applying a constant voltage of 3.3 V to the cartridge heater. Heating was continued until complete melting of the composite PCMs was achieved, allowing evaluation of their thermal buffering capacity and heat distribution characteristics.

The second experimental setup was designed to simulate one-dimensional heat flow through samples in response to a short burst of heat, replicating the thermal behaviour of the exothermic hydrogenation of a metal alloy. Specifically, the heat generated during $LaNi_5$ hydrogenation was emulated by varying the electrical input to the cartridge heater over time, from an initial peak to near zero. The input profile was derived based on the thermodynamics and kinetics of the hydrogen reaction forming $LaNi_5$, as reported in the literature [35, 36, 37], and is described as follows.

Ward et al. reported that the hydriding of $LaNi_5$ could be described by Equation 2, based on their experimental measurement of the enthalpy change associated with the reaction between hydrogen gas and $LaNi_5$ [36]:

$$(\frac{1}{3.1})LaNi_{5\,(cr)} + H_{2(g)} \rightleftharpoons (\frac{1}{3.1})LaNi_5H_{6.2\,(cr)} \quad (2)$$

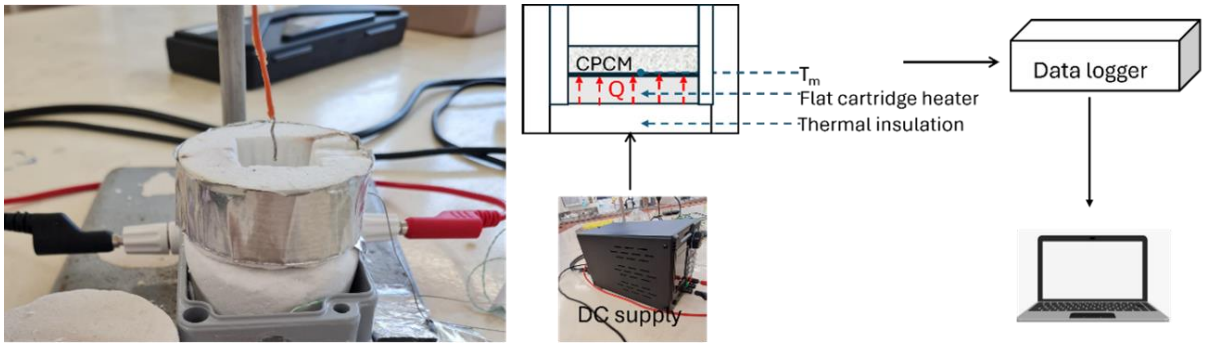

Figure 1. Thermal management performance test setup.

This reaction represents the formation of the hydride phase $LaNi_5H_{6.2}$ from $LaNi_5$ and hydrogen gas under near-atmospheric pressure. The stoichiometric coefficient of 1/3.1 reflects the molar ratio used in the experimental setup to normalize the reaction enthalpy per mole of hydrogen [36].

If the partial pressure of hydrogen remains almost constant, then the reaction may be assumed to be first order with respect to the non-reacted metal concentration according to the Johnson-Mehl-Avrami (JMA) model for $LaNi_5$ [37]. Assuming the reaction is first order with respect to $LaNi_5$ concentration and constant hydrogen concentration, then

$$\frac{d[x]}{dt} = -k[x] \tag{3}$$

Where:

- k is the rate constant, S^{-1}.
- [x] the concentration of $LaNi_5$.
- t is the reaction time, S.

Integrating both sides of Equation 3, we obtain (Equation 4).

Where:

$[x]_0$ is the initial concentration of $LaNi_5$.

$[x]_t$ is the concentration of $LaNi_5$ after a given time, t

Following the Arrhenius relationship between reaction rate and temperature:

$$k = Ae^{(-E_a/RT)} \tag{5}$$

Where:

- T is assumed as 311 K to match the temperature of the PCM.
- A is the pre-exponential factor for $LaNi_5$, equal to 1856 S^{-1}.
- E_a is the activation energy, 30.1 kJ/mol H_2 at near 1 atm.

So, refer to the following Equation 6.

Therefore, with the following Equation 7.

The enthalpy of reaction (2) is -99.5 ± 0.3 kJ·mol^{-1} (ΔrH_m^0), hence the heat released from the reaction per second is

$$Q = 99.5\ kJ \cdot mol^{-1} \times 0.0163\ S^{-1}[x]_0 e^{-0.0163t}$$
$$Q = 1.622[x]_0 e^{-0.0163t} \tag{8}$$

If we select an arbitrary initial concentration of $[x]_0$ = 6.17 M, we obtain the following equation for the rate of heat generated:

$$Q = 10e^{(-0.0163t)}\ \text{Watt} \tag{9}$$

The theoretical heat flux generated from $LaNi_5$, based on the above, along with the experimental applied heat flux, is shown in Figure 2. This calculated amount of heat generated from the reaction decreases exponentially over a short period. The experimental DC power was set up to deliver a power profile that matched this heat flux profile.

$$\int_{[x]_0}^{[x]_t} \frac{1}{[x]} dx = -\int_{t_0}^{t} kdt \implies \ln[x]_t = \ln[x]_0 - kt \implies [x]_t = [x]_0 e^{-kt} \tag{4}$$

$$k = 1856\ S^{-1} \times exp\left(-\frac{30.1 \times 1000\ J \cdot mol^{-1}}{8.314 J \cdot mol^{-1} \cdot k^{-1} \times 311K}\right) = 0.0163\ S^{-1} \tag{6}$$

$$[x]_t = [x]_0 e^{-0.0163t}\ or\ \frac{d[x]}{dt} = -0.0163[x]_0 e^{-0.0163t} \tag{7}$$

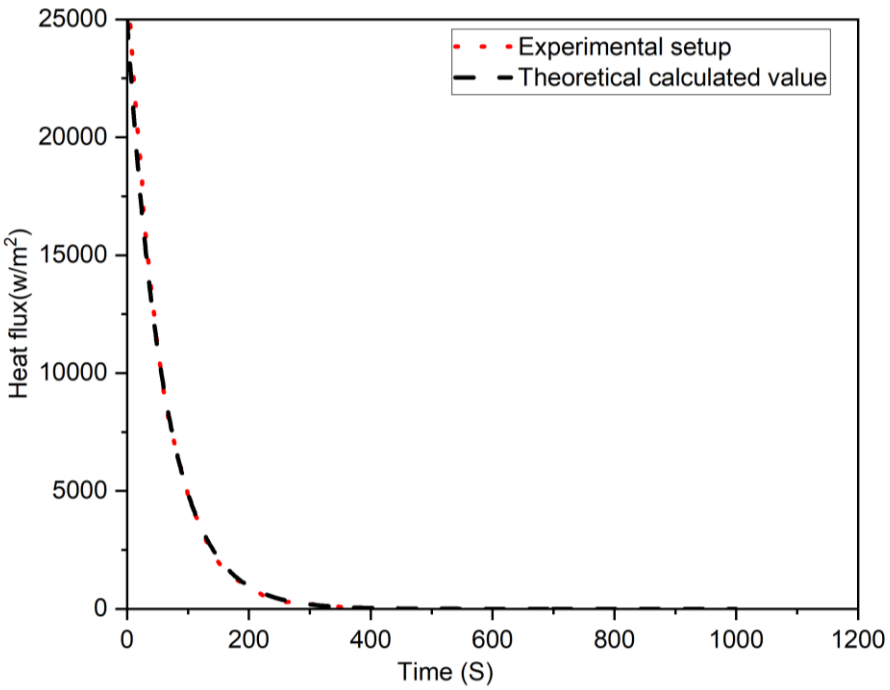

Figure 2. The calculated heat flux generated from hydrogenation of $LaNi_5$ and the current heat flux applied in this experiment.

RESULTS AND DISCUSSION

The morphology of cross-sections of the compressed expanded graphite matrix and its composite with paraffin is shown in secondary electron images (SEI) from SEM captured at an accelerating voltage of 15 kV and a magnification of 1200× (Figure 3). Figure 3a presents the typical morphological features of compressed expanded graphite. In contrast to pristine expanded graphite which typically exhibits a highly porous, loosely stacked, worm-like structure with large interlayer spaces [38], the compressed expanded graphite displayed a more compact and densified morphology due to the mechanical pressure applied during compression. Although the lamellar graphite structure remained discernible, the layers were pressed closer together, forming a more continuous and interconnected framework.

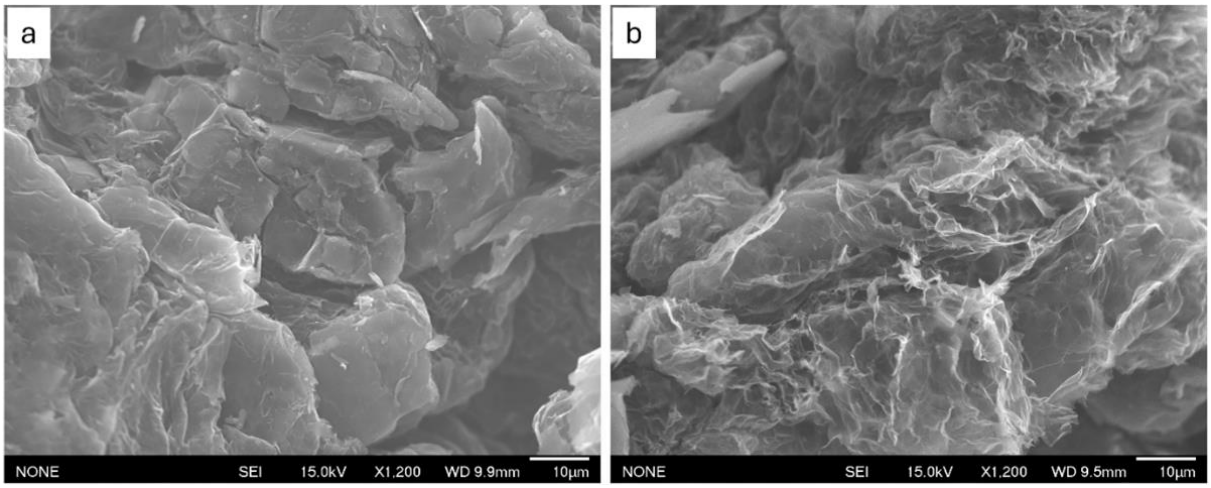

Figure 3. Secondary electron images (SEI) from SEM for (a) compressed expanded graphite matrix and (b) as-prepared composite PCM**.**

Figure 3b illustrates the morphology of the as-prepared graphite/paraffin composite after impregnation, revealing a more fibrous and porous structure that indicated successful paraffin infiltration. The graphite matrix exhibited excellent capillary adsorption capability, enabling the molten paraffin to effectively penetrate and occupy the interconnected pores within the graphite network. The overall porous architecture of the graphite was largely preserved after impregnation, suggesting that the capillary and adsorption forces were sufficient to fill the pores without inducing structural collapse. This retained structure formed a continuous graphite network that facilitated efficient thermal conduction pathways throughout the composite, thereby enhancing heat transfer performance while maintaining the high latent heat storage capacity of the paraffin.

The DSC melting curves of the pure paraffin PCM (PCM38) and graphite based composite PCM are shown in Figure 4, with the DSC curve of the pure paraffin PCM used as a reference. The melting curves of the composite PCMs exhibited similar shapes and peak positions to those of the pure PCM, indicating that the incorporation of graphite did not significantly affect the phase change temperature of the paraffin. The thermal properties derived from the DSC measurements are summarized in Table 1. The starting and ending temperatures of the melting transition for the composite PCMs closely matched those of the pure PCM, confirming that the thermal behaviour of paraffin was largely preserved within the graphite matrix.

The theoretical latent heat values of the composites were calculated using the latent heat of pure paraffin PCM38 and the measured paraffin mass fraction in the composites (~76 wt%). As expected, the composite PCMs exhibited a lower latent heat compared to the pure PCM, which was consistent with the composites having a paraffin content of approximately 76 wt%. The slight reduction in latent heat confirmed the presence of graphite as a thermally conductive skeleton that contributed negligible latent heat but provided continuous pathways for heat transfer. Similar results have been reported in the literature [32]. Importantly, the sharpness of the melting peaks indicated that the phase change process remained highly efficient, ensuring that the composites retained effective thermal energy storage performance.

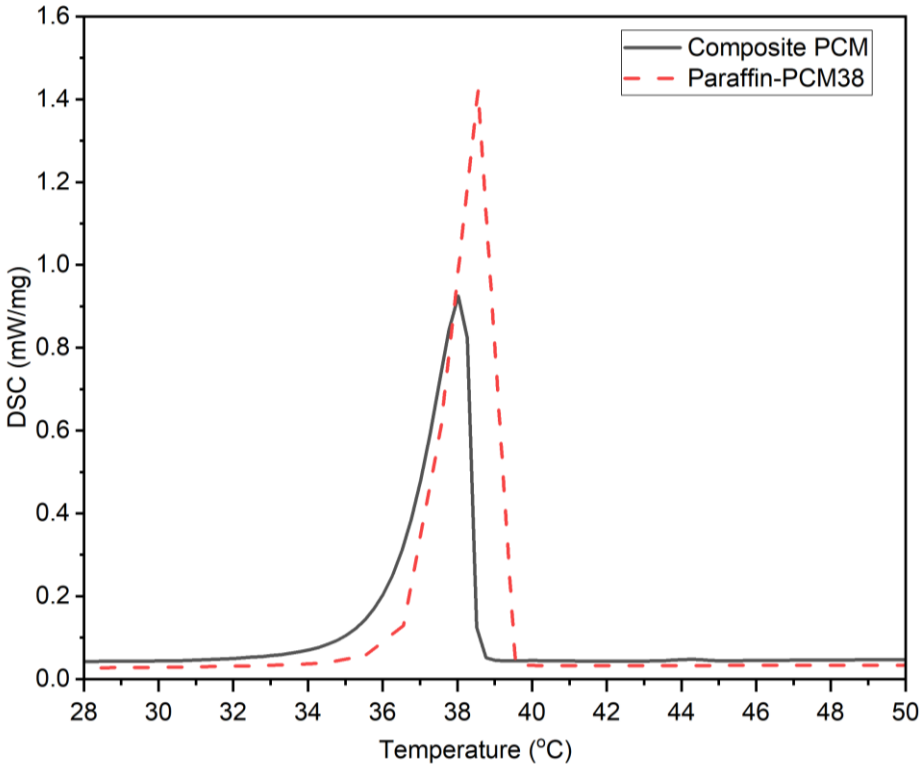

Figure 4. Melting DSC curves of the paraffin-PCM38 and graphite based composite PCM.

Table 1. Melting points and latent heat values of the paraffin and graphite based composite PCM.

Sample name	Starting (ºC)	Ending (ºC)	M.P. (ºC)	ΔH (J/g)	PCM loading mass %	Theoretical latent heat (J/g)[a]
Paraffin-PCM38	37.1	39.2	38.7	227	-	-
Graphite based composite PCM	36.3	38.4	38.1	170	76	173

[a] Theoretical latent heat was calculated using the latent heat values of pure paraffin-PCM38.

The influence of three composite PCM thicknesses (2.5 mm, 5.0 mm, and 10.0 mm) on thermal performance was studied under two different heat flux conditions. The thermal response was evaluated based on the temperature variation over time at the interface between the cartridge heater and the composite PCM, as this was the location that corresponded to the highest temperature region. The results are presented in Figure 5.

Figure 5a shows the surface temperature (T_m) profile during the application of a constant heat flux. As illustrated, the thinner composite PCM (2.5 mm) reached the PCM melting temperature much quicker (approximately 530 s) than the 5.0 mm (about 1000 s) and 10.0 mm (around 1820 s) samples.

The temperature plateau at approximately 37-38 °C observed in all three curves corresponded to the PCM melting period, during which latent heat was absorbed. As the PCM thickness increased from 2.5 mm to 10.0 mm, the duration of this plateau, and thus the effective heat absorption period, extended from about 470 s (2.5 mm) to 3250 s (5.0 mm) and 3680 s (10.0 mm). This indicates that thicker PCMs possessed greater latent heat storage capacity, allowing more thermal energy to be absorbed before complete melting. Consequently, thicker layers may maintain the metal hydride surface temperature below 40 °C for longer periods during hydrogenation, providing more stable thermal regulation and improved operational safety. In contrast, the thinner 2.5 mm PCM responded quickly but lost its heat absorption capability sooner, making it less effective for prolonged thermal control.

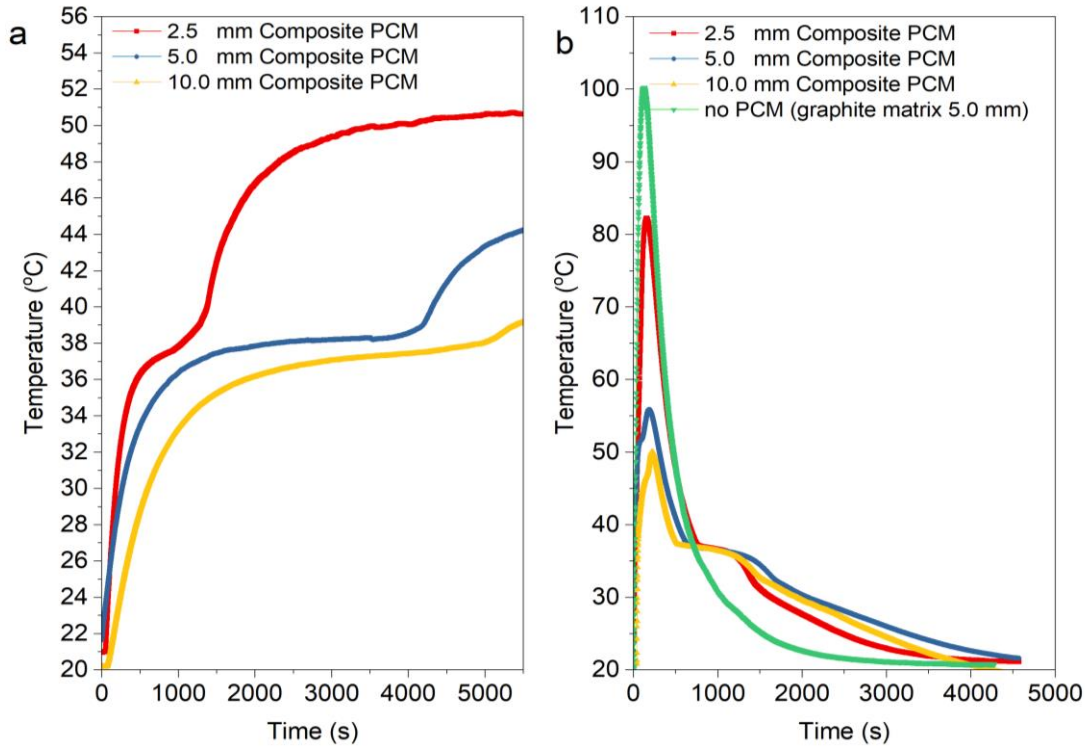

Figure 5. Effect of composite PCM thickness on the surface temperature, T_m, during heating (a) under a constant applied voltage of 3.3 V, and (b) application of an instantaneous heat flux.

On comparing the 5.0 mm and 10.0 mm samples, it is clear that doubling the thickness only slightly increased the plateau duration (from 3250 s to 3680 s), suggesting diminishing returns in heat absorption efficiency beyond a certain thickness. This indicates that while the thicker PCMs enhanced latent heat storage and prolong thermal buffering, excessively large thicknesses may compromise material efficiency and system compactness. Overall, the 5.0 mm PCM provided an optimal balance between heat absorption duration and design efficiency.

Figure 5b shows the surface temperature profiles of the 5.0 mm graphite matrix and graphite-based composite PCMs under a short heat flux. The results indicate that the graphite matrix reached its peak temperature faster than the composite PCMs. Although graphite possesses high thermal conductivity, which promotes rapid heat transfer, its low heat capacity limits its ability to store energy, leading to a faster surface temperature rise compared to the composite PCMs. Furthermore, the peak temperature decreased as the PCM thickness increased.

After heat input stopped, the graphite matrix exhibited a sharp temperature drop due to its limited heat storage capacity, whereas composite PCMs showed thermal lag, reflecting improved thermal buffering. The 2.5 mm PCM had a shorter lag than the 5.0 mm sample, and the 10.0 mm PCM also lagged less than the 5.0 mm, suggesting inefficient PCM utilization at higher thicknesses. Across all composite PCMs, the temperature stabilized at about 37–38 °C, corresponding to PCM melting and latent heat absorption.

Overall, a composite PCM thickness of 5.0 mm was found to provide the optimal balance between peak temperature reduction, thermal buffering, and latent heat utilization under the experimental conditions of this work. These results emphasise that PCM thickness optimization is crucial for achieving efficient heat transfer, effective latent heat storage, enhanced metal hydride system safety, and a compact, cost-effective system design.

CONCLUSION

This study demonstrated the potential of compressed expanded graphite-based composite PCMs for thermal management of hydrogen in metal hydrides operating at approximately 290–340 K and near-atmospheric conditions. The composite PCMs effectively regulated temperatures under both constant and short-burst heat fluxes. PCM thickness strongly influenced thermal response: thinner PCMs (2.5 mm) responded rapidly to heat flux, reaching peak temperatures quickly but providing limited latent heat storage and thermal buffering. Thicker PCMs slowed the temperature rise, reduced peak temperatures, and maintained the surface near the 37–38 °C latent heat plateau for longer, enhancing thermal regulation during hydrogenation. Increasing the thickness beyond 5.0 mm provided only marginal improvements, with the 10.0 mm PCM showing less efficient utilization. Overall, a 5.0 mm PCM achieved an optimal balance of rapid heat transfer, effective latent heat storage, thermal buffering, and operational safety for metal hydride systems. Future work will systematically investigate the effect of PCM thickness during dehydrogenation, under cycling conditions and with varying heat fluxes, to further optimize thermal lag, latent heat utilization, and overall heat transfer efficiency.

ACKNOWLEDGEMENTS

This work was supported by the Ministry of Business, Innovation and Employment (MBIE), New Zealand (Contract: UOWX2304).

REFERENCES

1. IEA (2025) Global energy review 2025. *IEA*, *Paris. Licence: CC BY 4.0.*

2. Kamran, M. and Turzyński, M. (2024) Exploring hydrogen energy systems: A comprehensive review of technologies, applications, prevailing trends, and associated challenges. *Journal of Energy Storage*, **96**, 112601.

3. Abe, J. O., Popoola, A. P. I., Ajenifuja, E. and Popoola, O. M. (2019) Hydrogen energy, economy, and storage: Review and recommendation. *International Journal of Hydrogen Energy*, **44(29)**, 15072–15086.

4. Tarhan, C. and Çil, M. A. (2021) A study on hydrogen, the clean energy of the future: Hydrogen storage methods. *Journal of Energy Storage*, **40**, 102676.

5. Mekonnin, A. S., Wacławiak, K., Humayun, M., Zhang, S. and Ullah, H. (2025) Hydrogen storage technology, and its challenges: A review. *Catalysts*, **15(3)**, 260.

6. Zarezadeh Mehrizi, M., Abdi, J., Rezakazemi, M. and Salehi, E. (2020) A review on recent advances in hollow spheres for hydrogen storage. *International Journal of Hydrogen Energy*, **45(35)**, 17583–17604.

7. Nemukula, E., Mtshali, C. B. & Nemangwele, F. (2024) Metal Hydrides for Sustainable Hydrogen Storage: A Review. *International Journal of Energy Research*, **2025**, 6300225.

8. Møller, K. T., Sheppard, D., Ravnsbæk, D. B., Buckley, C. E., Akiba, E., Li, H. W. & Jensen, T. R. (2017) Complex metal hydrides for hydrogen, thermal and electrochemical energy storage. *Energies*, **10**, 1645.

9. Qiao, L., Lu, C., Fan, W., Xue, Z., Wang, X., Kang, Z. & Sun, D. (2024) Metal-organic framework for hydrogen storage: Advances and challenges brought by the new technologies. In *International Journal of Hydrogen Energy*, **93**, 805–821.

10. Klopčič, N., Grimmer, I., Winkler, F., Sartory, M. & Trattner, A. (2023). A review on metal hydride materials for hydrogen storage. *Journal of Energy Storage*, **72**, 108456.

11. Chen, Y., Yong, H., Wang, S., Zhang, X., Zhang, W., Feng, K., Hu, J. and Zhang, Y. (2024) Hydrogen storage in Mg-Ni-type alloys with La and Sm incorporation. *ACS Applied Energy Materials*, **7(19)**, 8858–8868.

12. Bobet, J., Akiba, E., Nakamura, Y. & Darriet, B. (2000) Study of Mg-M (M=Co, Ni and Fe) mixture elaborated by reactive mechanical alloying — hydrogen sorption properties. *International Journal of Hydrogen Energy*, **25(10)**, 987–996.

13. Liu, Y., Chabane, D. and Elkedim, O. (2024) Optimization of LaNi5 hydrogen storage properties by the combination of mechanical alloying and element substitution. *International Journal of Hydrogen Energy*, **53**, 394–402.

14. Sato, T., Saitoh, H., Utsumi, R., Ito, J., Nakahira, Y., Obana, K., Takagi, S. and Orimo, S. I. (2023) Hydrogen absorption reactions of hydrogen storage alloy LaNi5 under high pressure. *Molecules*, **28(3)**, 1256.

15. Li, Q., Lu, Y., Luo, Q., Yang, X., Yang, Y., Tan, J., Dong, Z., Dang, J., Li, J., Chen, Y., Jiang, B., Sun, S. and Pan, F. (2021) Thermodynamics and kinetics of hydriding and dehydriding reactions in Mg-based hydrogen storage materials. *Journal of Magnesium and Alloys*, **9(6)**, 1922–1941.

16. Li, Y., Teliz, E., Zinola, F. and Díaz, V. (2021) Design of an AB5-metal hydride cylindrical tank for hydrogen storage. *International Journal of Hydrogen Energy*, **46(68)**, 33889–33898.

17. Davis Cortina, M., Romero de Terreros Aramburu, M., Neves, A. M., Hurtado, L., Jepsen, J. and Ulmer, U. (2024) The integration of thermal energy storage within metal hydride systems: A comprehensive review. *Inorganics*, **12(12)**, 313.

18. Manai, M. S., Leturia, M., Pohlmann, C., Oubraham, J., Mottelet, S., Levy, M. & Saleh, K. (2019) Comparative study of different storage bed designs of a solid-state hydrogen tank. *Journal of Energy Storage*, **26**, 101024.

19. Afzal, M. & Sharma, P. (2018) Design of a large-scale metal hydride based hydrogen storage reactor: Simulation and heat transfer optimization. *International Journal of Hydrogen Energy*, **43(29)**, 13356–13372.

20. Raju, M. and Kumar, S. (2012) Optimization of heat exchanger designs in metal hydride based hydrogen storage systems. *International Journal of Hydrogen Energy*, **37(3)**, 2767–2778.

21. Eisapour, A. H., Fung, A. S., Shafaghat, A. and Khosravi, K. (2025) Enhancing hydrogen storage efficiency in metal hydride tanks through conical heat exchangers and phase change material integration. *International Journal of Hydrogen Energy*, **109**, 1090–1107.

22. Shafiee, S. & McCay, M. H. (2016) Different reactor and heat exchanger configurations for metal hydride hydrogen storage systems - A review. *International Journal of Hydrogen Energy*, **41(22)**, 9462–9470.

23. El Mghari, H., Huot, J., Tong, L. and Xiao, J. (2020) Selection of phase change materials, metal foams, and geometries for improving metal hydride performance. *International Journal of Hydrogen Energy*, **45(29)**, 14922–14939.

24. Zhu, J., Lin, X., Lv, L., Li, M., Luo, Q., Kudiiarov, V. N., Liu, W., Leng, H., Han, X. & Ma, Z. (2024) The relationship between thermal management methods and hydrogen storage performance of the metal hydride tank. *Journal of Materials Science and Technology*, **203**, 66–77.

25. Tong, L., Xiao, J., Bénard, P. & Chahine, R. (2019) Thermal management of metal hydride hydrogen storage reservoir using phase change materials. *International Journal of Hydrogen Energy*, **44(38)**, 21055–21066.

26. Xu, Y., McCurdy, M. & Farid, M. (2025) The Use of Phase Change Materials for Thermal Management of Metal Hydride Reaction. *Applied Sciences*, **15(17)**, 9657.

27. Yazici, M. Y., Saglam, M., Aydin, O. & Avci, M. (2021) Thermal energy storage performance of PCM/graphite matrix composite in a tube-in-shell geometry. *Thermal Science and Engineering Progress*, **23,** 100915.

28. Ye, Y., Zhu, H., Cheng, H., Miao, H., Ding, J. & Wang, W. (2023) Performance optimization of metal hydride hydrogen storage reactors based on PCM thermal management. *Applied Energy*, **338**, 120923.

29. Kumar Rajamony, R., Chinnasamy, S., Kamaraj, R. & Mohanthy, A. (2025) Thermal Performance Enhancement of Phase Change Material using Coconut Shell Biochar for Sustainable Thermal Energy Storage. *Malaysian Journal of Chemistry*, **27**, 353-360.

30. Poosapadi, D., Papade, C. V., Suthan, R., Manohara, M. & Manoj Kumar, P. (2025) Characterization Studies on a Nano-doped Organic Phase Change Material for Improving Thermal Energy Storage. *Malaysian Journal of Chemistry*, **27**, 472-480.

31. Zhu, S., Nguyen, M. T. & Yonezawa, T. (2021) Micro- and nano-encapsulated metal and alloy-based phase-change materials for thermal energy storage. *Nanoscale Advances*, **3(16)**, 4626–4645.

32. Al-Shannaq, R. & Farid, M. M. (2018) A novel graphite-PCM composite sphere with enhanced thermo-physical properties. *Applied Thermal Engineering*, **142**, 401–409.

33. Alassaad, K., Minto, J. & de Wilde, P. (2025) Enhancing Building Thermal Performance: A Review of Phase Change Material Integration. *Energies*, **18**, 3200.

34. Nizovtsev, M. I. & Sterlyagov, A. N. (2024) Effect of phase change material (PCM) on thermal inertia of walls in lightweight buildings. *Journal of Building Engineering*, **82**, 107912.

35. Kumar, S., Kojima, Y. and Dey, G. K. (2018) Thermodynamics and kinetics of hydrogen absorption–desorption of highly crystalline LaNi5. *Journal of Thermal Analysis and Calorimetry*, **134**, 889–894.

36. Ward Hubbard, B. N., Rawlins, P. L., Connick, P. A. & Stedwell, R. E. (1983) The standard enthalpy of formation of $LaNi_5$, The enthalpies of hydriding of $LaNi_{5-x}Al_x$. *Journal of Chemical Thermodynamics*, **15**, 785–798.

37. Muthukumar, P., Satheesh, A., Linder, M., Mertz, R. and Groll, M. (2009) Studies on hydriding kinetics of some La-based metal hydride alloys. *International Journal of Hydrogen Energy*, **34**, 7253–7262.

38. Oya, T., Nomura, T., Tsubota, M., Okinaka, N. & Akiyama, T. (2013) Thermal conductivity enhancement of erythritol as PCM by using graphite and nickel particles. *Applied Thermal Engineering*, **61(2)**, 825–828.